Engineering Science and Technology, an International Journal 62 (2025) 101966

Contents lists available at ScienceDirect

Engineering Science and Technology, an International Journal

journal homepage: www.elsevier.com/locate/jestch

Numerical prediction of strength and temperature changes within cemented paste backfill considering barricade stability

Di Wu [a], Liang Liu [a], Erol Yilmaz [b,*], Shilong Zheng [a]

[a] School of Civil and Resource Engineering, University of Science and Technology Beijing, Beijing, China
[b] Department of Civil Engineering, Geotechnical Division, Recep Tayyip Erdogan University, Fener, Rize TR53100, Turkey

ARTICLE INFO

Keywords:
Barricade
Lateral pressure
Cemented paste backfill
Temperature
Coupled model

ABSTRACT

Manufacturing an intended recipe of tails, binder and water, cemented paste backfill (CPB) is employed to refill the cavities created in underground mining operations. To ensure that it remains stable and forms a solid structure, filling slurry must be supported by a rigid barricade at the bottom of the mining area. Fill structures' process is guided via coupled thermal/hydraulic/mechanical/chemical developments, which can directly affect the stability of barricade. Hence, it is essential to study the pressure changes and distribution within the barricade. A fully coupled THMC numerical model was established in the current study in order to predict mechanical features and temperature changes inside CPB, and to measure effect of these changes on barricade's stability. Predictive outcomes obtained from the model built were compared with the results of a field experiment, showing good consistency and thus proving model's validity in mimicking evolution of temperature change and its effect on strength features of barricade in the course of backfill hydration. The verified multi-physical field model was used to numerically study the change of lateral pressure of barricade under different working conditions. The results show that properly increasing the initial temperature of CPB and increasing the distance between the barricade and the stope can effectively alleviate the lateral pressure on the barricade. The consequences of the existent research could offer a vital guideline on the topic of backfill barricade's stability analysis.

1. Introduction

Through the unceasing enlargement of society/economy, call for ore assets is gradually growing, and concurrently, ore deposits' mining has also caused a great effect on ecosystem, leaving a large number of underground openings. To realize green and smart mining, cemented paste backfill (CPB) has become a mainstream technology [1]. CPB is a tail/cement/water mix, which is employed to back-fill mining spaces, improve the surface stability, reduce the surface collapse, and expand ore's recovery rate [2]. After backfill slurries are filled into stope, they are in paste form. To ensure that they can remain in place and form a solid structure, barricade becomes an integral fragment of filling method. As filling slurries continue to fill, pressure on the barricade increases, so the strength and stability of barricade is a key factor in filling design [3,4].

In response to the above problems, numerous scholars have embarked on research on barricade [5–7]. Cui and Fall [8] clinched that lateral pressure on barricade is ruled by multifaceted physical developments in filling, covering coupled thermal/hydraulic/mechanical/chemical practices, and established a multi-physical coupled model for the curing process of cement-based materials such as CPB [9–11]. Cement's hydration reaction contributes to fill's consolidation, and its lateral pressure on the barricade stops growing as backfill cures over time [12]. The binder is exothermic in the hydration process, and the heat it releases causes the growth of thermal stresses within fill, and water consumed within cement hydration process and drainage process through the barricade also cause changes in the lateral pressure of barricade [13–15]. Wang et al. [16] investigated the influence of curing pressure on bottom CPB stability considering diverse barricade types. Zhai et al. [17,18] explored computable link between CPB's lateral load and effect of waste rock barricade, and estimated a 3D methodical explanation regarding waste rock barricade.

* Corresponding author at: Geotechnical Division, Department of Civil Engineering, Recep Tayyip Erdoğan University, Zihni Derin Campus, Fener, Rize TR53100, Turkey.
E-mail addresses: DiWu1218@ustb.edu.cn (D. Wu), liuliang@xs.ustb.edu.cn (L. Liu), erol.yilmaz@erdogan.edu.tr (E. Yilmaz), zhengshilong@xs.ustb.edu.cn (S. Zheng).

https://doi.org/10.1016/j.jestch.2025.101966
Received 30 July 2024; Received in revised form 16 December 2024; Accepted 16 January 2025
Available online 20 January 2025
2215-0986/© 2025 The Author(s). Published by Elsevier B.V. on behalf of Karabuk University. This is an open access article under the CC BY-NC-ND license (http://creativecommons.org/licenses/by-nc-nd/4.0/).

To appreciate change of lateral stress of barricade more intuitively, several scholars have studied changing rule of stress on barricade during filling by means of on-site measurements or indoor preparation of similar physical models [19,20]. Wang et al. [21] investigated the lateral pressure change of barricade during filling by burying pressure sensors inside the retaining wall. The results of field measurements showed that the lateral pressure of barricade initially augmented progressively by rising fill height and approached the maximum value. Thompson et al. [22] installed earth stress sensors within backfill and barricade to scrutinize links between fill's internal pressure and barricade's lateral pressure. Doherty et al. [23] measured total/pore water pressure inside the backfill of three different stope, it was determined that the filling interval had the most significant effect for the lateral pressure of barricade during and after filling. These field measurements provide insight into the influencing factors related to the lateral pressure of barricade.

Although in-situ measurements of the lateral pressure of barricade can directly show the pattern of pressure change, the in-situ measurements affect the normal production of the mine as well as requires a lot of time to monitor the in-situ data [24–26]. Numerical simulation has the advantages of high efficiency and low cost compared with in-situ measurements, and a variety of coupling models have been established to simulate CPB's coupling behavior [27–29]. For example, Cui and Fall [30,31] established a completely coupled THMC model of CPB to simulate the changing of material properties under multi-physical field condition. Wu et al. [32,33] developed an in-situ model of hydraulic/mechanical performance of filling to mimic the evolution of hydraulic behavior of filling subjected to in-situ conditions along with slurry fill and hydration. However, these models did not consider fill's coupled behavior and its effect on barricade during long-time continuous filling process [34,35]. Thus, in this paper, a numerical model making an allowance for the influence of THMC coupling process within backfill will be developed and analyzed lateral pressure change of fill's barricade and internal temperature, and issues influencing barricade's lateral pressure will be investigated by using the model.

The objective of this study is to make a contribution to the optimal design and reliable stability analysis of the barricade. The principal objective of this study is to develop a numerical model that considers the impact of the THMC coupling process on the long-term continuous filling process of the CPB. Additionally, the study aims to numerically examine the lateral pressure change of the barricade under varying filling conditions.

2. THMC model

2.1. Hydration equation

To designate hydration's evolution, concept of degree of hydration reaction $\eta(t)$ is hosted to indicate cement hydration reaction's degree at the moment t. Cement hydration's process is signified below [36]:

$$\eta(t) = \eta_u \cdot \exp\left[-\left(\frac{\theta}{t}\right)^{\alpha} \right] \tag{1}$$

where θ and α are hydration reaction parameters at situation heat; η_u is cement hydration's final degree, and t is cement hydration's reaction time.

Considering temperature impact on hydration reaction, the time t at different CPB temperatures is converted into the equal time t_e at situation heat, and the corresponding time t_e could be stated below:

$$t_e = \int_0^t \exp\left[\frac{E_a}{R}\left(\frac{1}{T_r+273} - \frac{1}{T_c+273}\right)\right] dt \tag{2}$$

where E_a is stimulation energy; R is common gas continual; T_r is temperature; T_c is fill's heat.

E_a/R is cement's activation heat which could be further stated below:

$$\frac{E_a}{R} = \xi\left(\frac{30}{T_c+10}\right)^{0.39} \tag{3}$$

where ξ is the activation temperature at the situation heat, which is 4600 K.

Cement hydration's final degree can be further expressed as:

$$\eta_u = \frac{1.031r}{0.194+r} \leqslant 1 \tag{4}$$

where r is a value of mass rate of water and cement used within filling and r is 6.258 for a maximum final hydration of cement of 1.

2.2. Heat equation

Fill's temperature change is directly linked to exothermic binder hydration and heat conduction between fill and setting [37]. Hydration reaction's exothermic rate could be expressed below:

$$Q(t) = Q_\infty \left(\frac{\theta_c}{t}\right)^{\alpha} \cdot \left(\frac{\alpha \cdot \theta_c}{\theta \cdot t}\right) \cdot \eta(t) \cdot \xi \cdot \left(\frac{30}{T_c+10}\right)^{0.39} \cdot \left(\frac{1}{T_r+273} - \frac{1}{T_c+273}\right) \tag{5}$$

where $Q(t)$ is hydration reaction's exothermic rate; Q_∞ is heat ultimately generated via hydration reaction; θ_c is hydration reaction parameter at CPB's own temperature.

As fill interacts with nearby rock, heat transfer between two surfaces is known as convective heat [32]:

$$q = \frac{\partial T}{\partial t} = \gamma t (T_c - T_r) \tag{6}$$

where q is the convective heat; T_c is fill's surface temperature; T_r is nearby rock's heat; γ is convective heat coefficient between fill and nearby rock (Kj/m^2•℃); and t is the medium convection time.

Any object with a temperature above absolute zero possesses a heat transfer mode that sends thermal radiation to the outside world. Therefore, during fill's hydration reaction, development of thermal radiation between CPB and the external surrounding rock is considered below:

$$q_r = \varepsilon C_s \left[(T_c+273)^4 - (T_r-273)^4 \right] \tag{7}$$

where ε is the essential surface emissivity with a value in the range of 0.85–0.95; C_s is the Stefan-Boltzmann constant (5.67×10^{-8}W, m^2•K^4).

2.3. Fluid flow equation

Darcy's law was utilized to define the apparent velocity of CPB pore water during filling [38–40]:

$$u = \frac{Kk_i}{\rho g} \nabla(\rho g - p) \tag{8}$$

where u is pore water flow rate; ρ is fill's density; k_i is relative permeability; K is fill's saturated permeability; p is fill's pore water pressure.

K value drops with cement hydration and is given by the equation below [41,42]:

$$K = K_T \exp\left(-8.173\eta^{4.035}\right) \tag{9}$$

where K_T is tailings' saturated permeability.

$$k_i = \sqrt{\omega}\left[\int_0^{\omega} \frac{1}{h(x)} dx \Big/ \int_0^1 \frac{1}{h(x)} dx \right]^2 \tag{10}$$

Where $h(x)$ is stress head; ω is dimensionless water content (see the equation below):

Table 1
Input limits, edge circumstances and primary values.

Parameters	Value
Initial CPB temperature (℃)	25
external temperature (°C)	25
CPB density (kg/m^3)	1711
Cement density (kg/m^3)	1310
CPB Poisson's ratio	0.2
λ_r	0.12
k_i	0.6
K	1
γ	1.3
K_{di}	1
k_d (1/h)	0.02
c_i (MPa)	1
δ	0.013
τ	125
φ	30
machine module	
top surface	free
lateral surface	roller support
bottom surface	fix
volume force	gravity
thermal module	
top surface	convective heat
lateral surface	convective heat
bottom surface	convective heat
hydraulic module	
top surface	entrance
lateral surface	wall
bottom surface	wall
volume force	gravity

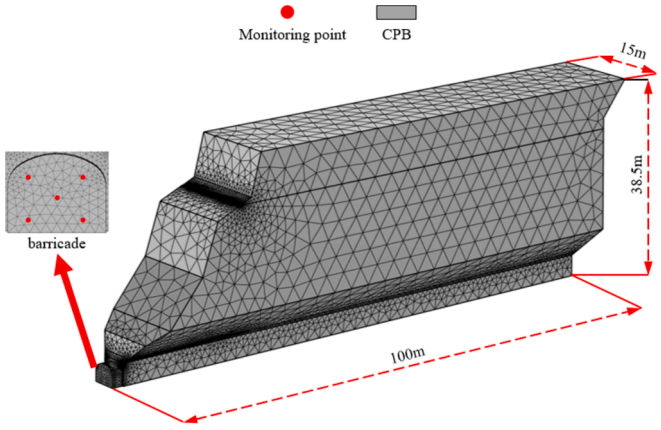

Fig. 1. Grid division results of the stope.

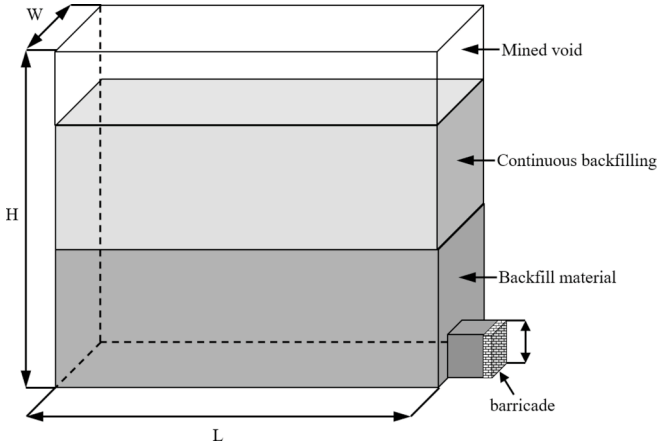

Fig. 2. Structure of continuous filling.

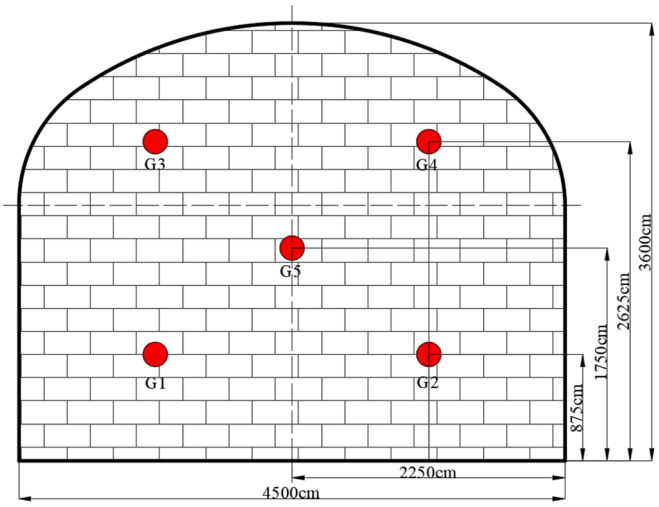

Fig. 3. Arrangement and distribution of sensors on the barricade.

$$\omega = \frac{\lambda - \lambda_r}{\lambda_s - \lambda_r} \tag{11}$$

where λ is fill's water content; λ_s and λ_r are saturation and residual values of fill's water content.

2.4. Mechanical equation

The horizontal pressure of CPB at depth H could be stated below:

$$p_h = \frac{\nu}{1-\nu}\left(\rho g H - \Phi p \sigma_{ij}\right) \tag{12}$$

where ν is fill's Poisson's rate; σ_{ij} is Kroenecker's delta function; $\sigma_{ii} = 1$; $\sigma_{i \neq j} = 0$.

For the CPB, the heat is generated by the hydration process of the binder, which creates thermal stress within the CPB, and the chemical shrinkage is caused by binder reacts with water. In addition, when the CPB structure is placed in the underground stope for ground support, it will be subjected to the stress of the surrounding rock, resulting in the elastic–plastic deformation of the CPB. Therefore, based on the above discussion, the total stress of the CPB structure should include elastic, plastic and thermal stresses as well as chemical shrinkage.

$$\varepsilon = \varepsilon_{el} + \varepsilon_{pl} + \varepsilon_{th} + \varepsilon_{ch} \tag{13}$$

where ε is the total strain, ε_{el}, ε_{pl} and ε_{th} are the elastic, plastic and thermal strains respectively, and ε_{ch} is the chemical shrinkage.

To simplify the modelling, the CPB structure is assumed to be isotropic and the constitutive relationship between the effective stress and the elastic strain of CPB is expressed as follows:

$$\sigma_{eff} = D\varepsilon_{el} = D\left(\varepsilon - \varepsilon_{pl} - \varepsilon_{tl} - \varepsilon_{ch}\right) \tag{14}$$

where: σ_{eff} is effective stress; and D is elastic matrices.

Considering change in bulk modulus of CPB with time under the effect of hydration reaction, fill's bulk modulus could be stated below as a role of equal agfe:

$$K_d = K_{di}[\lambda_d - (\lambda_d - 1)\exp(-k_d t_e)] \tag{15}$$

where K_{di} is early bulk modulus before hydration; λ_d is rate of peak bulk modulus to initial value; k_d is rate of alteration of bulk modulus by hydration reaction.

CPB's shear modulus could be expressed below:

$$G_d = \frac{3K_d(1-2\nu)}{2(1+\nu)} \tag{16}$$

Fig. 4. Sensor installation process. (a) Earth pressure sensor; (b) Processing of the sensor; (c) Fixing of the sensor in the barricade; (d) Completion of the sensor installation.

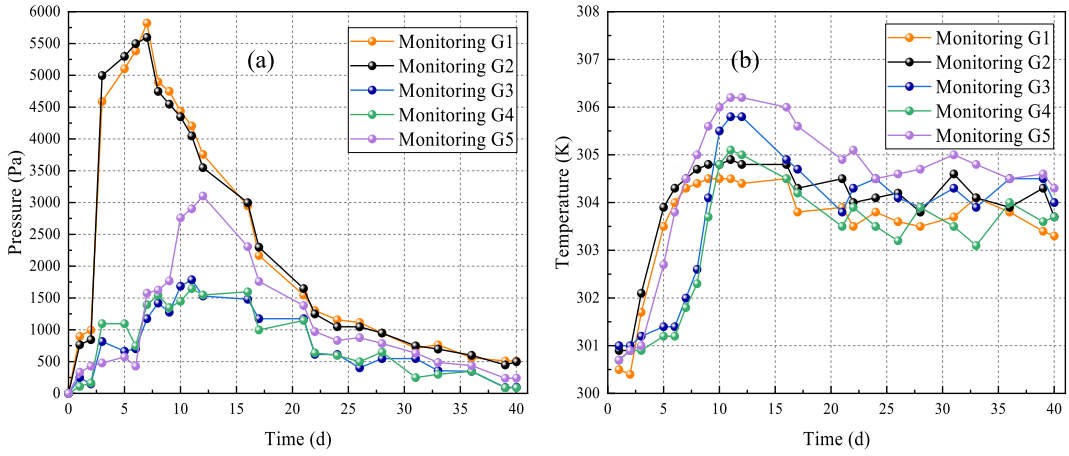

Fig. 5. Lateral pressure variation on barricade and temperature variation inside CPB: (a) Pressure monitoring; (b) Temperature monitoring.

Considering CPB's plastic behavior, the following equation is used to express its plastic deformation:

$$f = \alpha_p I_1 + \sqrt{J_2} - k_p \tag{17}$$

where I_1 is initial stress invariant; J_2 is second unbiased stress variable.

α_p and k_p are yield function parameters, which can be expressed by Mohr-Coulomb criterion matching using the following equation:

$$\alpha_p = \frac{2\sin\varphi}{\sqrt{3}\cdot(3-\sin\varphi)} \tag{18}$$

$$k_p = \frac{2\sqrt{3}c\cos\varphi}{3-\sin\varphi} \tag{19}$$

where c is fill's cohesion; φ is fill's internal friction angle.

During fill's hydration, cohesion c varies continuously with hydration reaction (see equations below):

$$c = c_i[\tau - (\tau - 1)\exp(-\delta t_e)] \tag{20}$$

where c_i is CPB cohesion of initial hydration; τ is ratio of extreme cohesion to initial cohesion; δ is changing rate of cohesion with hydration.

Through the evolution process of the hydration degree of binder with time, the hydration reaction equation, the thermodynamic equation, the hydraulic equation and the mechanical equation can be combined to form a coupling model. Since the hydration degree of binder changes with temperature, the coupling model is dynamically dependent on temperature and time.

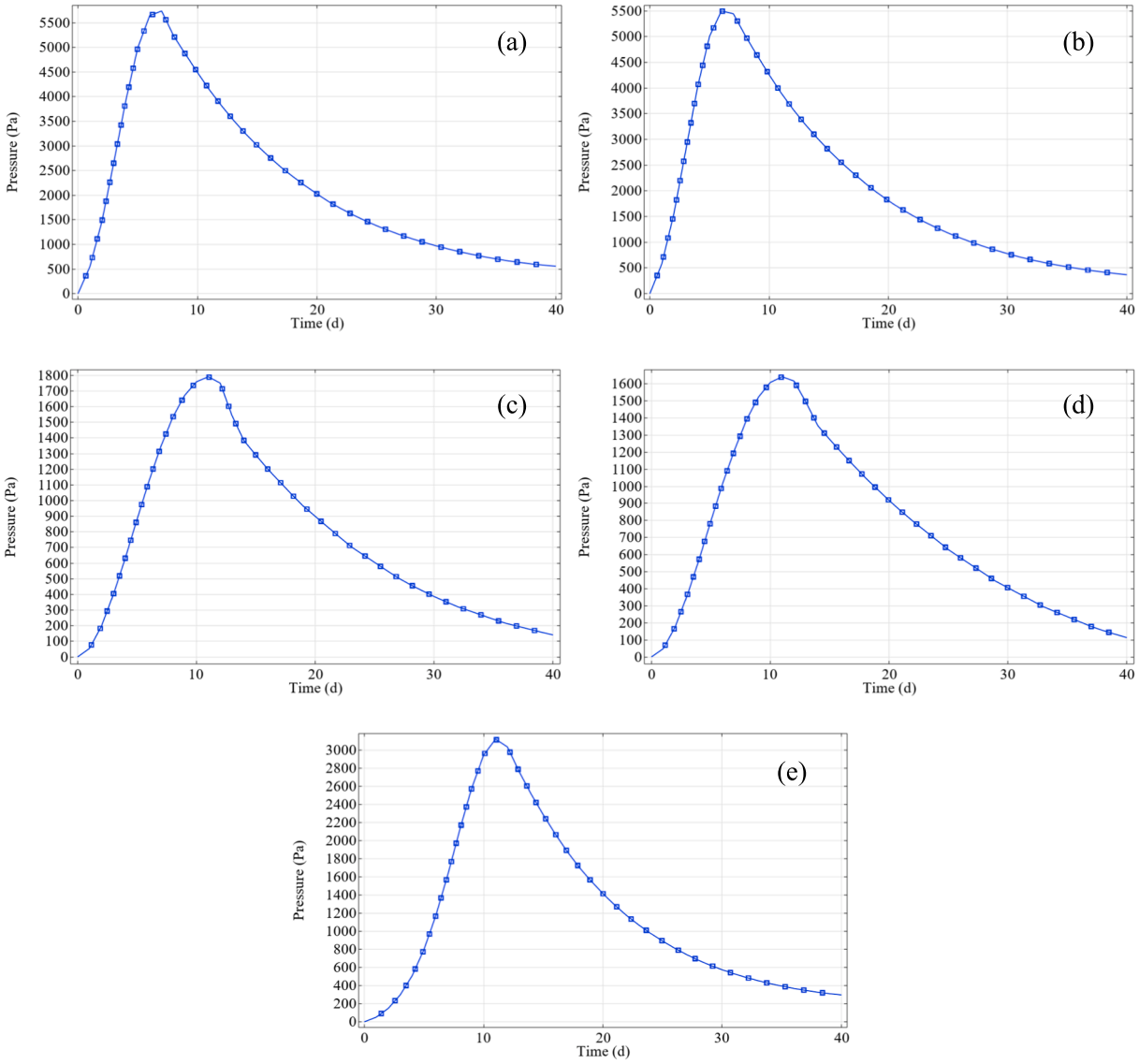

Fig. 6. Simulation of lateral pressure change on barricade with time for different sensor locations: (a) G1; (b) G2; (c) G3; (d) G4; (e) G5.

3. Validation of the model

To confirm feasibility of established mathematical model and its ability to foresee barricade's strength properties, model validation was carried out through finite-element software COMSOL Multi-physics, importing established model into COMSOL Multi-physics, and selecting in-situ data of an iron ore mine site monitoring for comparison via model simulation outcomes. Table 1 shows input limits, primary values and edge circumstances for model confirmation.

After importing the established 3D geometric model of the quarry into COMSOL Multiphysics, the model is meshed after inputting linked equations, limits and initial values (Fig. 1). This results in a total of 1,029,038 domain units, with a minimum unit mass of 0.0035 and an average unit mass of 0.6885.

3.1. Introduction to the stope

An iron ore mine adopts the whole tailing filling slurry to continuously fill mined-out openings, fill's concentration is 68 %, and cement/tail rate is 1:7. Fig. 2 shows 3D schematic diagram of goaf's filling process, and the stope's width/height/length is 15 m/38.5 m/100 m, because the filling slurry is in the "black box maintenance" state after being filled into the stope. Since fill is in the "black box maintenance" state after filling into stope, to analyze the change rule of barricade pressure in fill's diverse stages, the earth stress sensor is fixed in barricade, to measure barricade's pressure change and change rule of temperature at different filling heights.

Before filling the stope, to monitor the overall situation of lateral stress on barricade, a total of five measurement sensors were arranged at different heights of the barricade for this monitoring. The bottom and top sensors are arranged symmetrically along the center line of barricade, distance between G1 and G2 with the bottom floor of barricade is 0.875 m, and space between them with barricade's side wall is 1.125 m; similarly, the distance between the top earth pressure sensors G3 and G4 with the bottom floor of barricade is 2.625 m, and the distance between them with barricade's center line is 1.125 m; the middle earth stress sensor G5 is arranged in barricade's center line, and space between it with barricade's bottom floor is 1.75 m. Fig. 3 directs its detailed planning. After determining the location of measurement points, sensor is fixed in barricade's internal structure by steel wire. Fig. 4 shows detailed installation practice.

During filling, lateral stress change of each sensor and fill's internal temperature change are shown in Fig. 5. The lateral pressure data measured by the sensor can be seen, with rising fill height, lateral stress

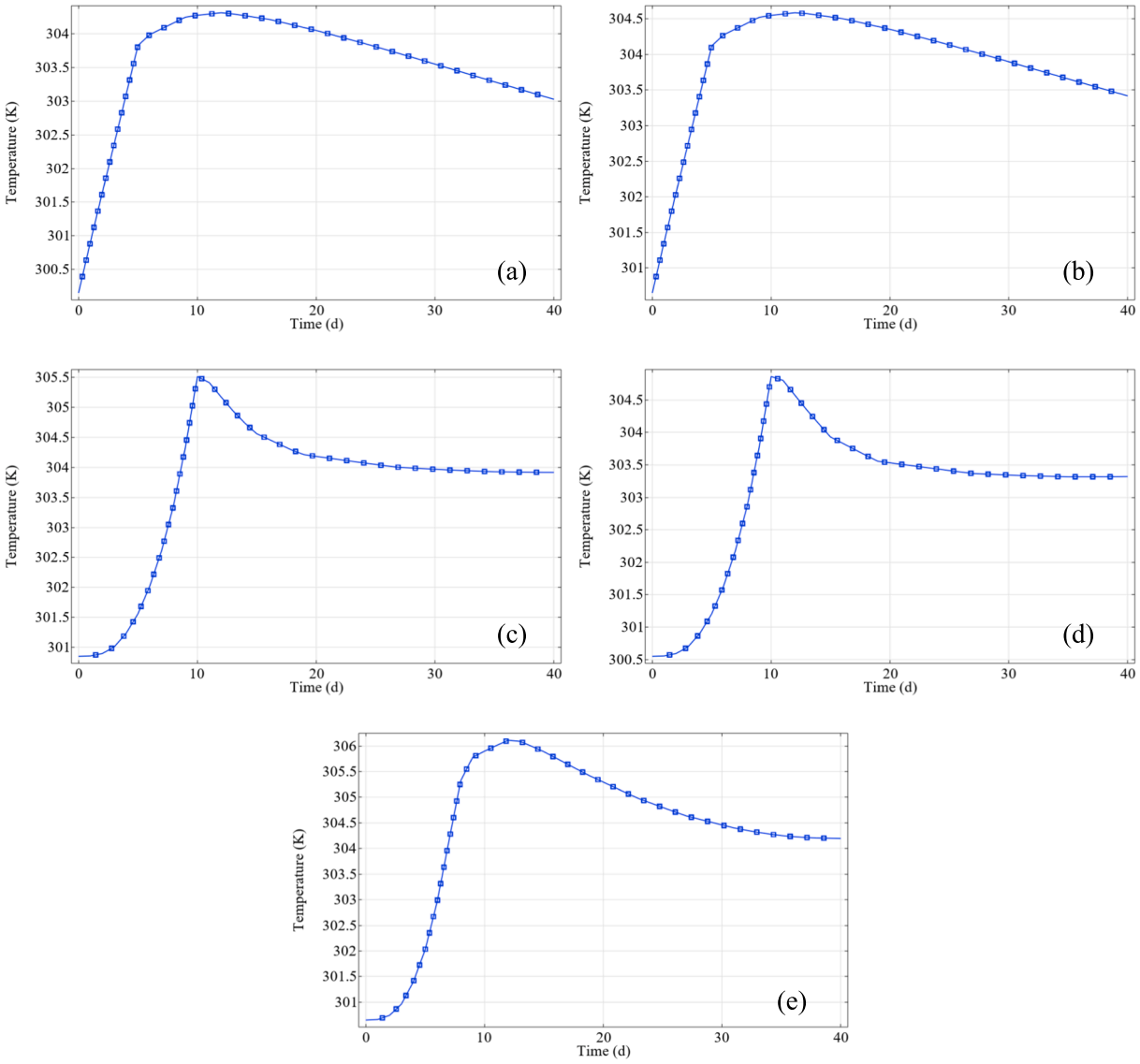

Fig. 7. Simulation of internal temperature of CPB with time for different sensor locations: (a) G1; (b) G2; (c) G3; (d) G4; (e) G5.

on barricade firstly surges and then cuts, and lastly tends to stabilize, analyze reason for this change is that at the beginning of filling, fill slurry has not yet formed a cured structure, which will cause a certain degree of lateral pressure, and with the increase in filling height after a certain period of time, CPB forms a cured structure to bear the pressure of the upper filling slurry. At the same time, due to CPB has a certain self-supporting and self-shrinkage phenomenon, so that the lateral pressure gradually becomes smaller.

The temperature data measured by the sensor can be seen, the temperature inside CPB is also the first to rise to the peak, after reaching the peak gradually reduced to stabilize. Analyzing reason for the change is early fill's hydration reaction lasts to carry out, made a large amount of heat, with the increase in maintenance time, hydration reaction is weakened, temperature is reduced, but due to hydration reaction has made more heat, so the temperature after stabilization is higher relative to the initial temperature.

3.2. Model simulation and verification

Confirm model's validity, monitoring facts agreeing to in-situ measurements are agreed on barricade of constructed 3D model to record and display the data of lateral pressure on barricade and fleeting change of temperature in CPB. The monitoring points, which correspond to the field measurements, are arranged on the geometric model of CPB. and the simulation time was the same as the actual filling time (Fig. 6).

From the simulation results of lateral stress, once can see that lateral stress in early stage is increasing with time, after reaching the peak begins to fall and stabilizes. The trend of the temperature simulation results is also roughly the same, the internal temperature of CPB with the increase in time continues to increase, after a period of time to reach the peak, and then begins to gradually fall, and stabilizes. It is basically the same trend as the measured data. From simulation outcomes, one could establish that peak time of the lateral stress monitored by the measurement points at different heights is different, and the peak time monitored by the measurement points at the bottom is earlier, and the peak value is larger. There is not much difference in the time to peak temperature and peak values between the different monitoring point locations, and the temperature peak at the bottom measurement point is not the largest, unlike the lateral pressure trend.

After filling into stope, to clearly show impact of different filling heights in stope on barricade's lateral pressure, slicing in the longitudinal direction along the centerline of stope. The lateral pressure distribution inside CPB at diverse filling heights can be seen in Fig. 7. In fill's early stages, barricade's lateral stress mainly comes from impact of

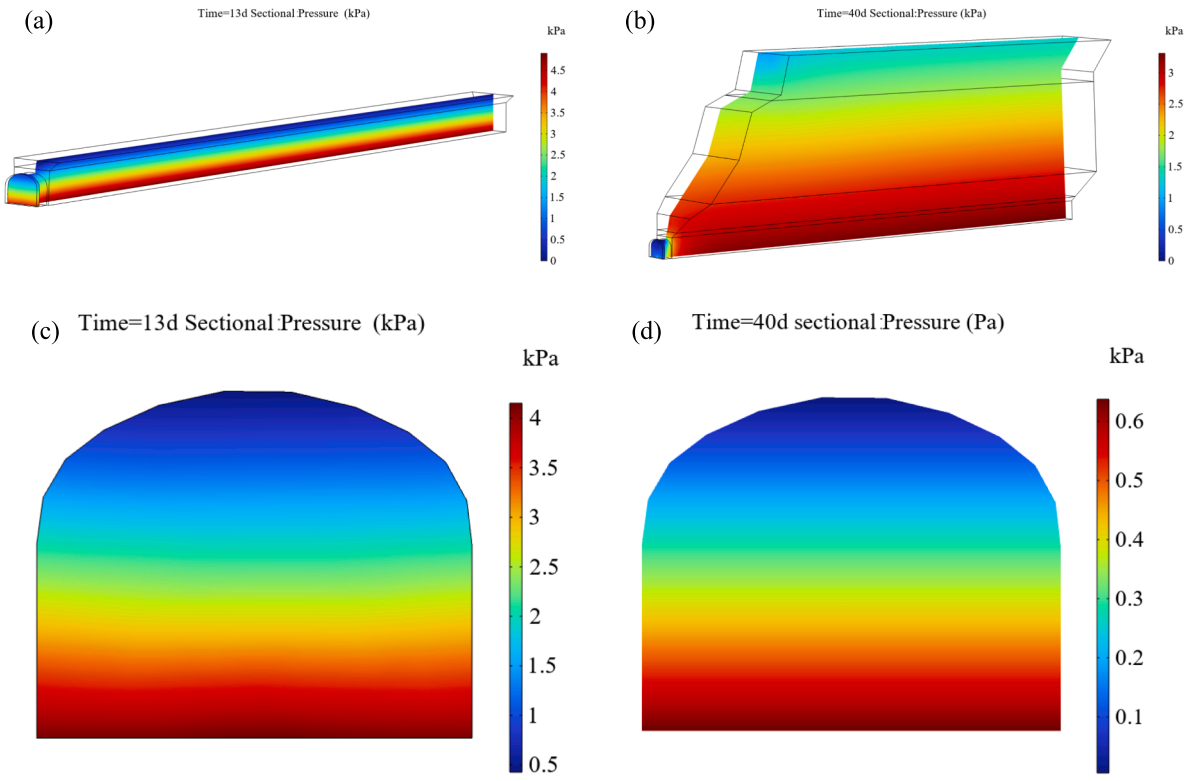

Fig. 8. Simulation of pressure distribution at CPB internal cross-section and barricade after filling 13-day and 40-day. (a) CPB internal cross-section after filling 13-day; (b) CPB internal cross-section after filling 40-day; (c) barricade after filling 13-day; (d) barricade after filling 40-day.

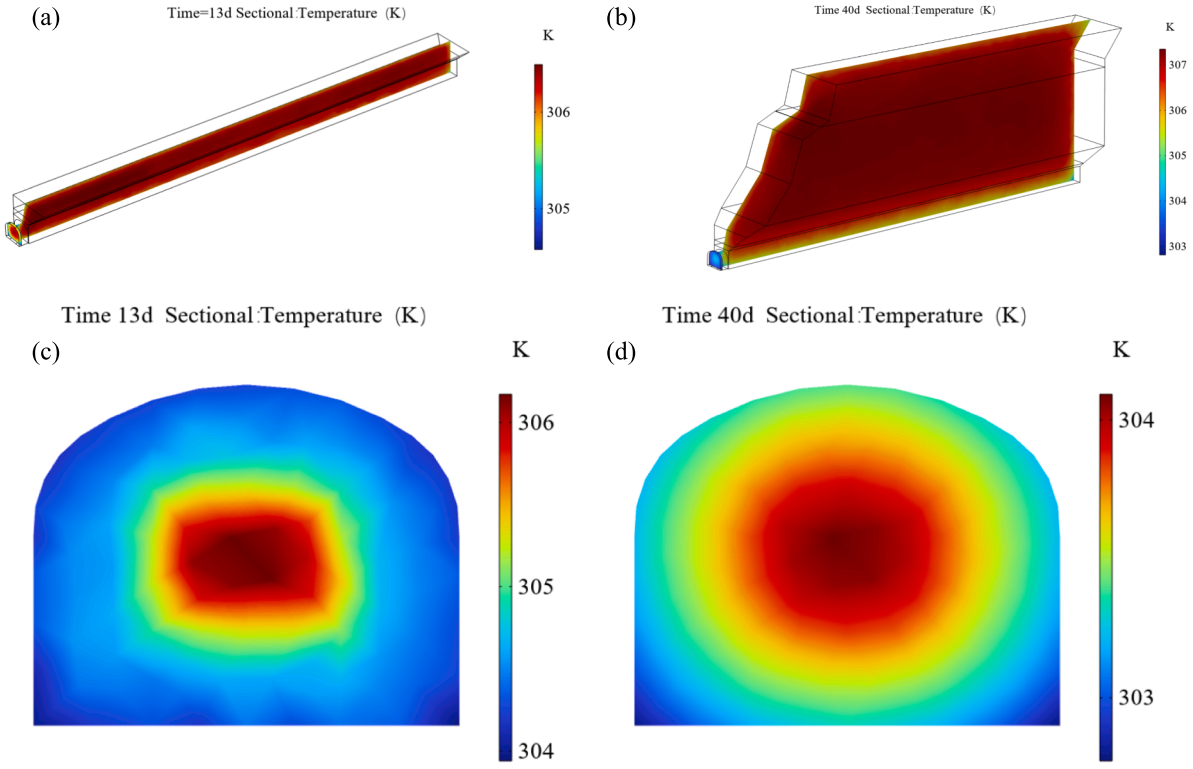

Fig. 9. Simulation of temperature distribution at CPB internal cross-section and barricade after filling 13-day and 40-day. (a) CPB internal cross-section after filling 13-day; (b) CPB internal cross-section after filling 40-day; (c) barricade after filling 13-day; (d) barricade after filling 40-day.

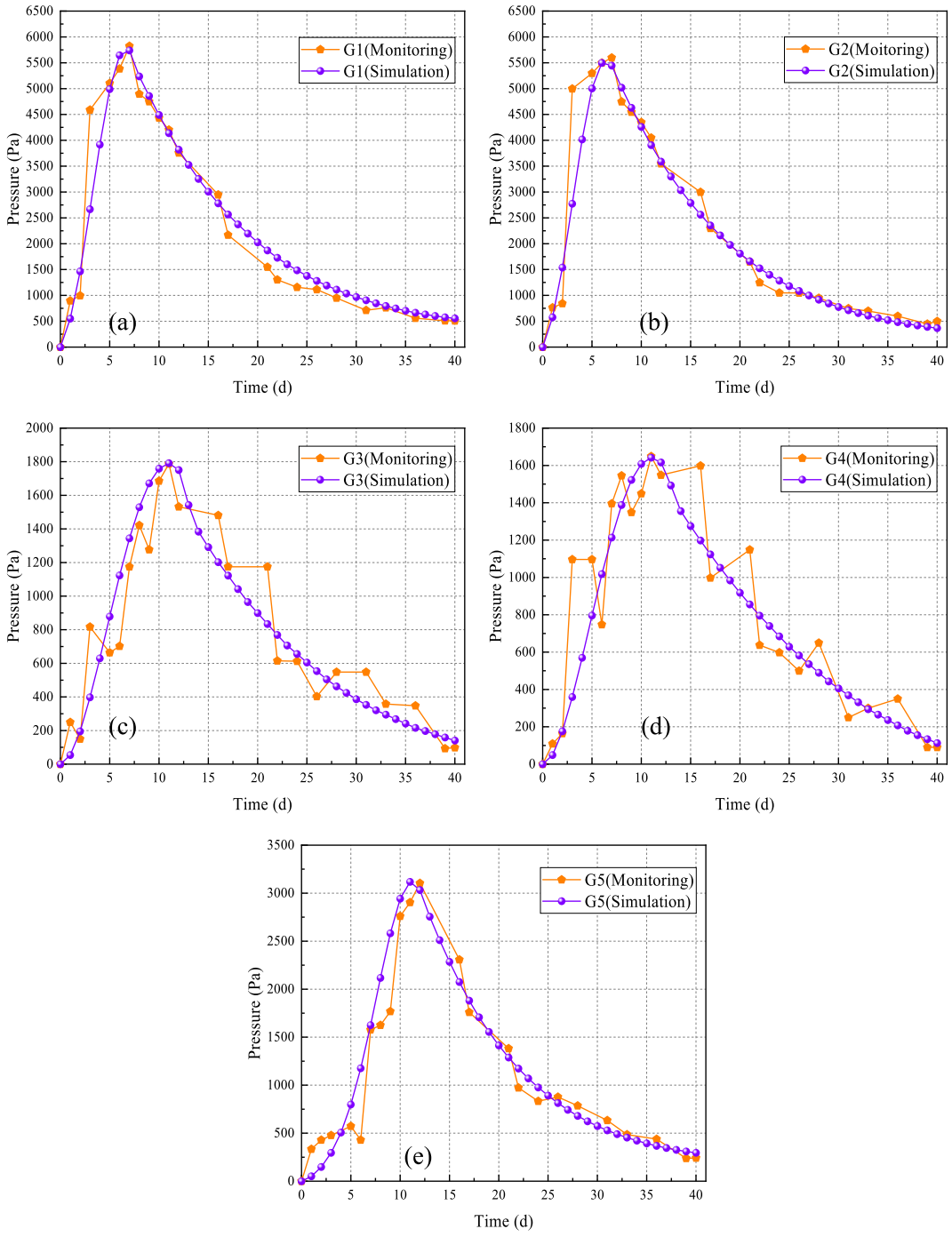

Fig. 10. Comparison of simulated lateral pressure data with monitoring data at different sensor locations: (a) G1; (b) G2; (c) G3; (d) G4; (e) G5.

filling slurry on barricade, at this time the filling slurry is in the state of loose fluid, filling slurry in this state will exert maximum pressure on the barricade. Due to the different heights of the measurement points, the time to reach the peak lateral pressure at each measurement point is different, and as barricade's lateral stress reaches an extreme value, with increase of fill height, the bottom of CPB is basically cured, the strength is gradually formed, and the lateral pressure on the barricade gradually decreases.

From Fig. 8, we can observe the distribution of the temperature inside CPB and on the barricade at different filling heights. In the early stage of filling, the humidity inside CPB is larger than that at the edge, and the hydration reaction is more intense, In the initial phase of the CPB curing process, the hydration of the binder generates a considerable amount of heat, which results in a rapid rise in the CPB temperature. Subsequently, as a consequence of the deceleration of the hydration process of the binder and the heat exchange between the CPB and the surrounding environment, the CPB temperature declines until it reaches a state of stability (approaching ambient temperature). and at the same time, the heat in CPB is slower to be dissipated compared with that at the edge. Hence, the heat at barricade's center is greater than one of the edge. From the results obtained, one could witness that coupled model can well designate change of lateral pressure on the barricade and the change rule of temperature inside CPB.

To further confirm coupled model's validity, simulated data are exported and matched by the field monitoring data (Fig. 9). By comparing simulation and monitoring data on barricade in Fig. 9, one

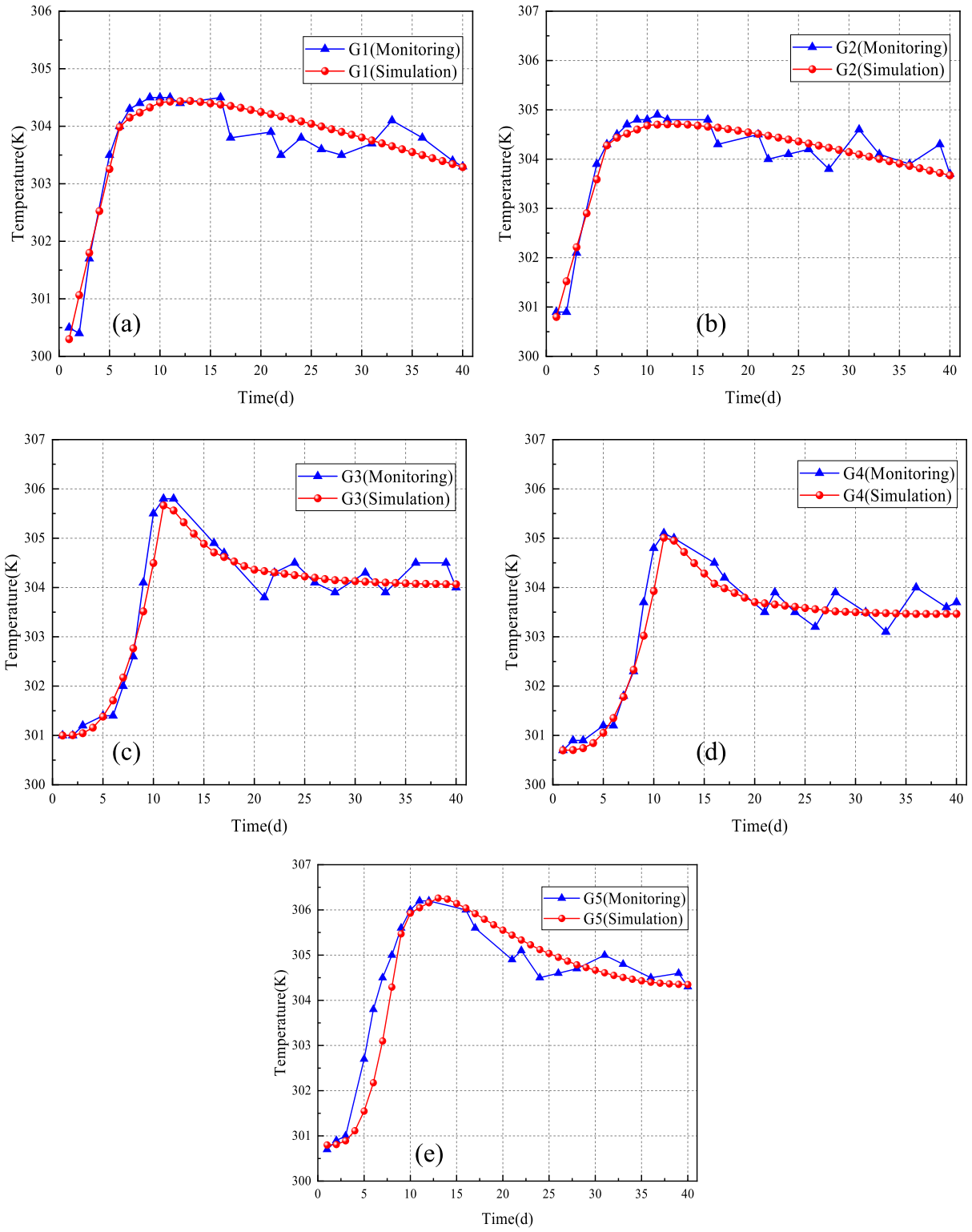

Fig. 11. Comparison of simulated temperature data with monitoring data at different sensor positions: (a) G1; (b) G2; (c) G3; (d) G4; (e) G5.

can conclude that coupled model could well describe lateral pressure change process of barricade with time, and simulation results' trend and monitoring results are basically the same. From the comparison of the lateral pressure change outcomes, one could see that, whether it is monitoring outcomes or the simulation results, the trend of the lateral pressure change is that rises to the peak value in the early filling period and then decreases slowly, and finally tends to stabilize. Comparing the heat simulation data with the monitoring data at different monitoring points, it can be found that the internal temperature change of CPB under the simulation is the same as the monitoring data, which further verifies coupled model's validity in simulation of internal heat change rule at the process of fill's hydration reaction. The error of some data may be caused by the change of boundary conditions (Fig. 10).

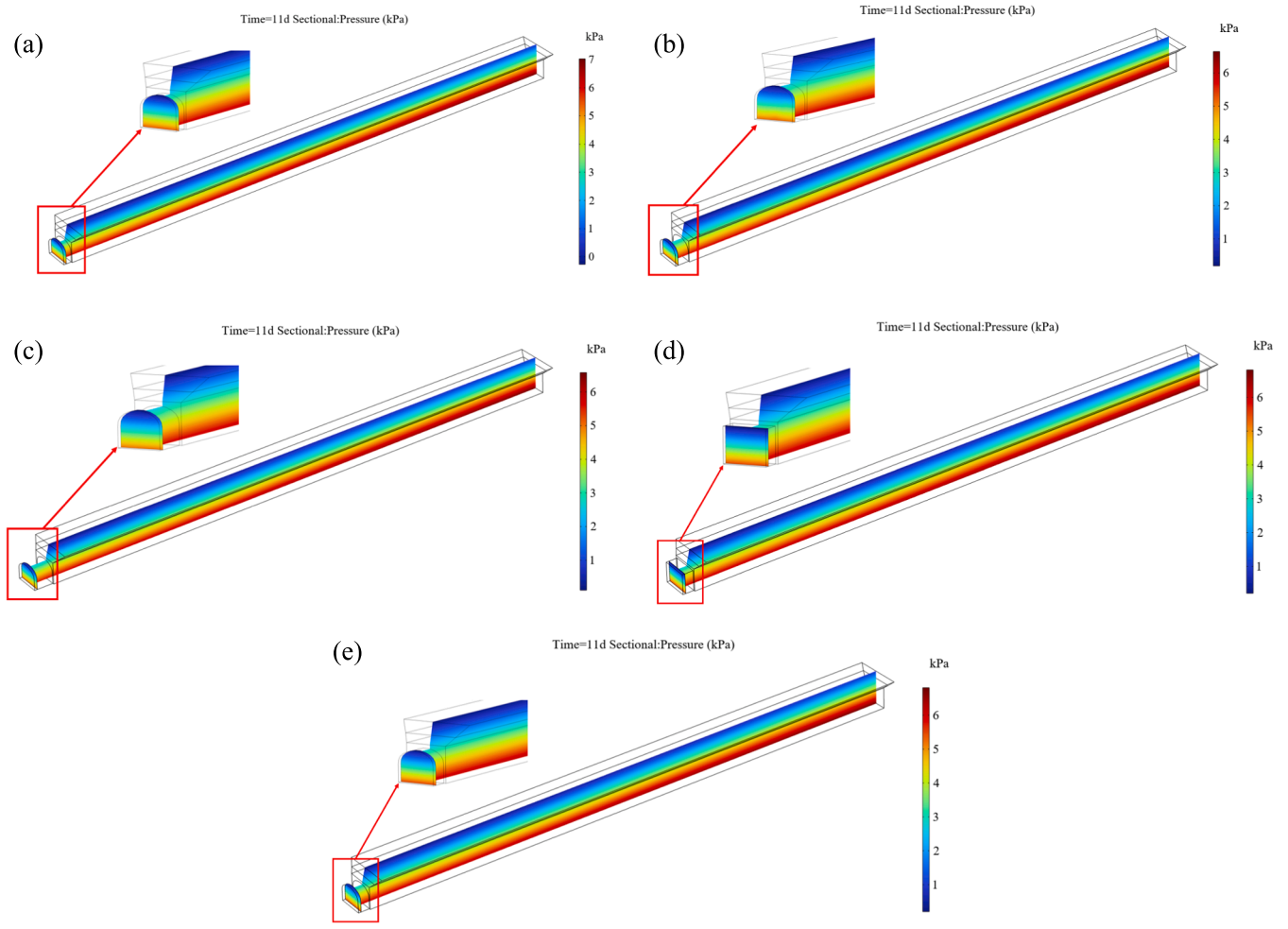

Fig. 12. Pressure distribution in CPB for different placements and shapes of barricade. (a) 1 m distance; (b) 2 m distance; (c) 3 m distance; (d) rectangular barricade; (e) arch barricade.

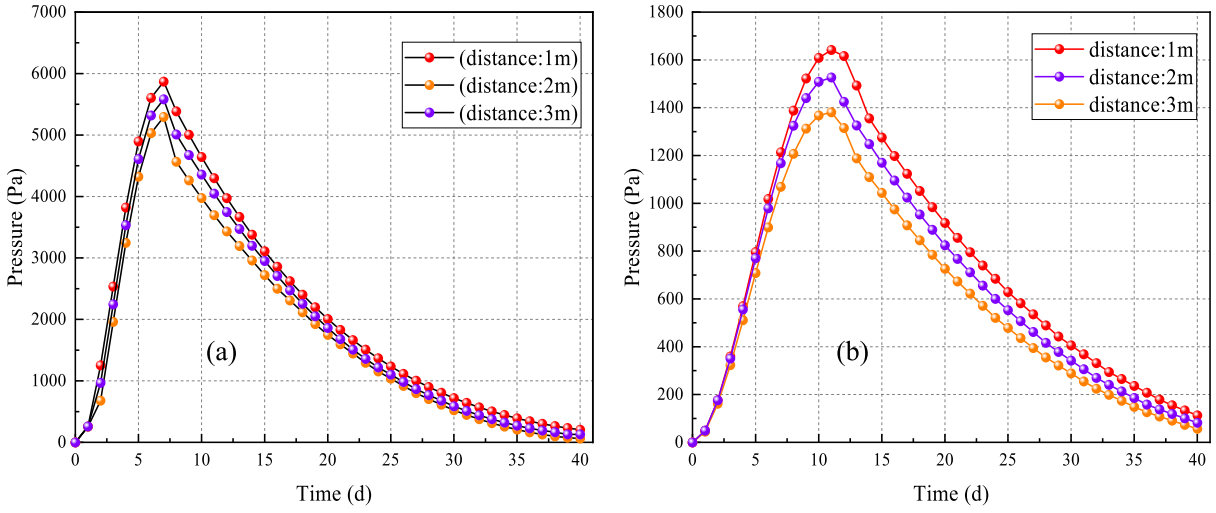

Fig. 13. Comparison of simulated lateral pressures at G2 (a) and G4 (b) with different barricade placements.

4. Implementing the model

Simulation outcomes show that established model could foresee changes of lateral stress on barricade and the internal temperature of CPB under the influence of coupled multi-physics fields. As the initial temperature of the CPB increases, the internal curing rate of the CPB also rises, resulting in the CPB entering the consolidation state at a faster rate. As a result of temperature dependence of hydration process,

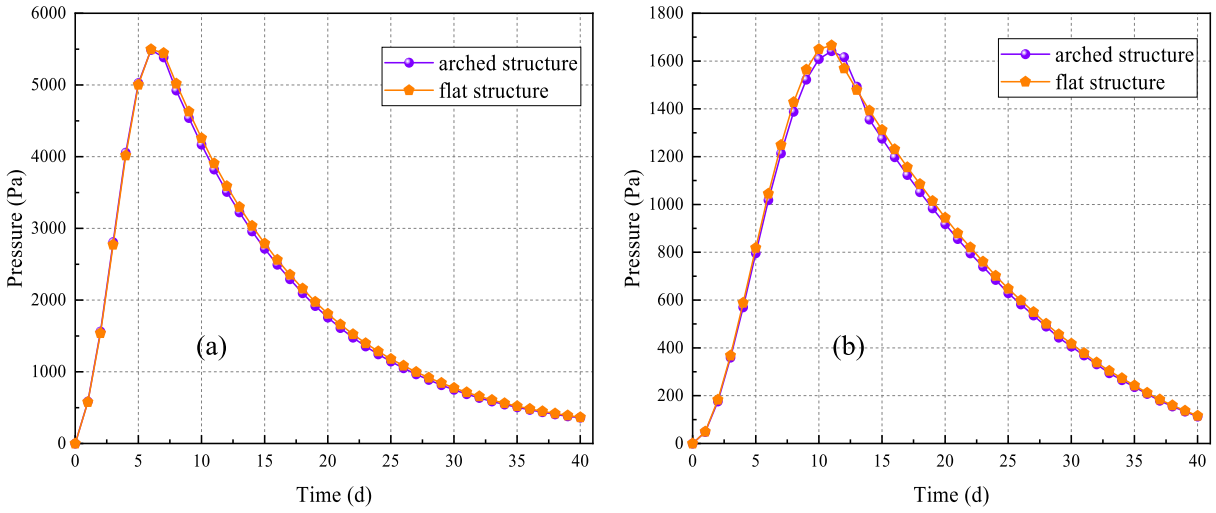

Fig. 14. Comparison of simulated lateral pressures at G2 (a) and G4 (b) with different shapes.

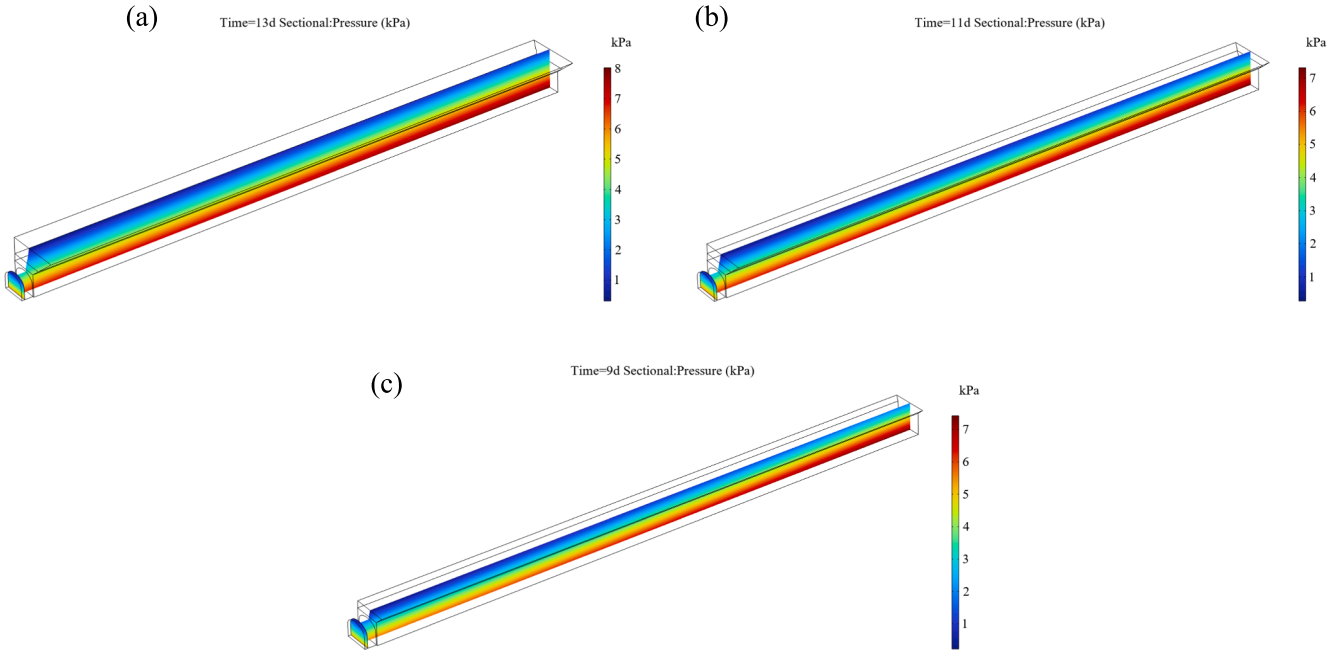

Fig. 15. Pressure distribution inside CPB at different CPB initial heats: (a) 10 °C, (b) 25 °C, and (c) 40 °C.

changing of fill's initial temperature will affect change in the coupled behavior of the THMC inside CPB, which in turn has an impact for the change of the lateral pressure on barricade [43–45]. At the same time, different placement positions of the barricade and the shape of the barricade also have a corresponding effect for the lateral pressure change on the filled baffle wall, and different consistencies of filling slurry can also affect the lateral pressure on the barricade. Thus, it is necessary to use established model to explore the impacts of different placement positions and shapes of barricade and different CPB initial temperatures and different filling slurry concentration for barricade's lateral pressure.

Space between barricade and stope is set to 1 m, 2 m and 3 m respectively, and the shape of the barricade is changed to rectangle based on the original model, to study the impact of diverse placement and shape of barricade for change of lateral stress on barricade. Effect of different fill temperatures for lateral stress change on barricade is considered, observe effect of fill in 10 °C, 25 °C and the 40 °C for lateral stress on barricade. Considering effect of diverse fill slurry concentrations, observe the effect of 66 %, 68 % and 70 % concentrations for lateral stress on barricade (Fig. 11).

4.1. *Effect of barricade placements and shapes*

Since G1, G2 are at the same height, the change trend is basically the same, the same to G3 and G4. so only use the change of lateral pressure on the barricade at the position of G2 andG4. Fig. 12 displays specific pressure circulation in CPB for different locations and shapes of barricades. Fig. 13 indicates that when barricade is out of the stope, lateral pressure on barricade is smaller, as barricade is 3 m and 2 m out of stope, compared to the distance of 1 m, the overall trend of the pressure change is basically the same, and the overall pressure is relatively lower, especially obvious at the peak. The main reason is that the bottom of the CPB is basically in a consolidated state at 11 days of curing. As the distance between the barricade and the stope increases, the influence of

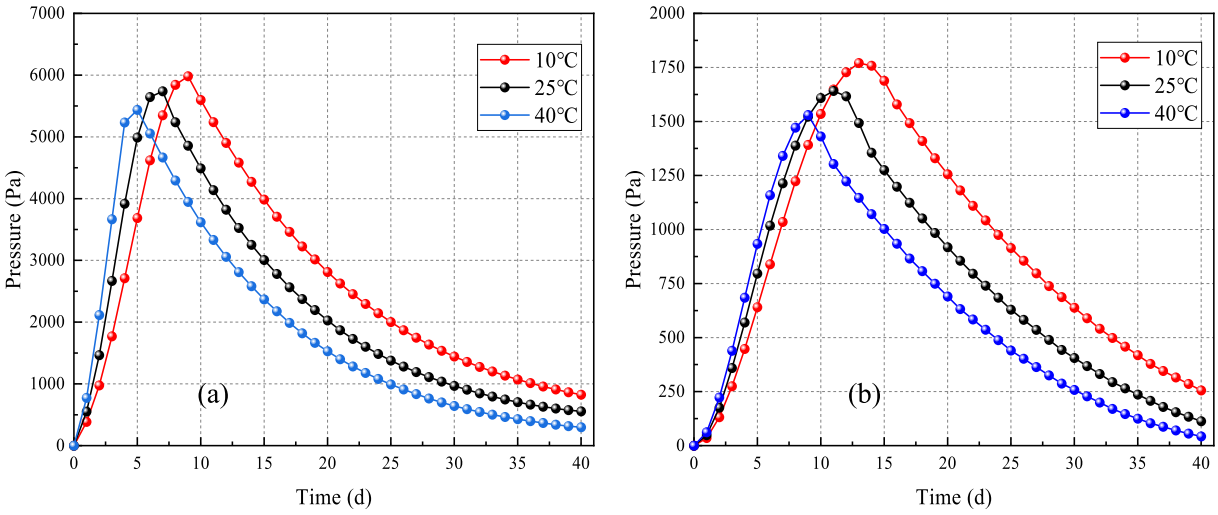

Fig. 16. Comparison of lateral pressure at G2 (a) and G4 (b) with different CPB initial temperatures.

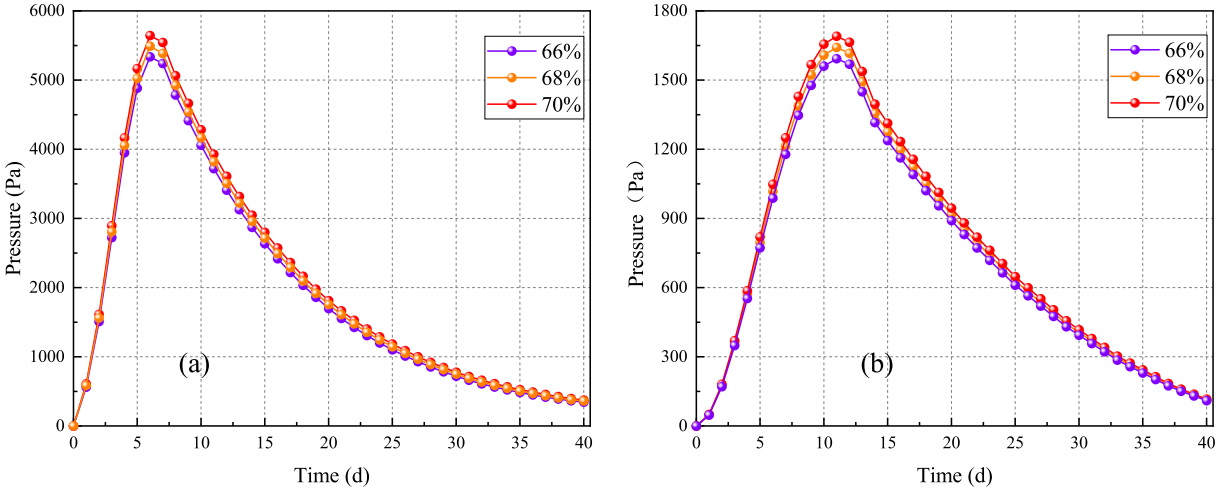

Fig. 17. Comparison of lateral pressure at G2 and G4 with different slurry concentrations. (a) G2; (b) G4.

local load on the lateral pressure of the barricade becomes smaller and smaller, and the distance increases to a certain extent. Increasing the distance has no obvious effect on reducing the lateral pressure of the barricade. Therefore, in the process of barricade design, the location of the barricade should be fully considered. Avoid placing the barricade close to the mouth of the stope and try to place it twice the height of the barricade from the mouth of the stope, which will effectively reduce the lateral pressure on the barricade. From Fig. 14, it can be noticed that the shape of the barricade is designed as a rectangle, the lateral pressure on the barricade is almost unchanged compared with the arch-shaped barricade, indicating that the influence of the shape of the barricade on the lateral pressure for the barricade is negligible.

4.2. *Effect of CPB initial temperature*

Fig. 15 shows the pressure distribution inside fill at diverse fill initial heats. Fig. 16 indicates the effect of diverse CPB heats on lateral pressure of barricade, as fill's initial temperature surges, time for the lateral pressure of the barricade to reach the maximum value will be earlier, and at the same time the pressure will be reduced. When the initial temperature of CPB is 40℃ or 25℃, the peak of lateral pressure at G2 will reach earlier, but the overall trend is basically the same without too much change. While the initial temperature is 10℃, the peak will reach relatively later. It is found that the increase of temperature will make the lateral pressure on barricade to reach its peak earlier and the value of pressure peak is relatively low.

The leading aim for this occurrence is that higher initial temperature of CPB will accelerate fill's hydrated reaction, so that it will be cured quickly, shorten the original curing time, and quickly form the early strength. Due to the bottom plate effect, the bottom CPB can bear stress brought by superior fill slurry, thereby relieving pressure on barricade [46–48]. Thus, new curing methods, such as microwave curing, can be used to heat CPB to reduce the lateral pressure of CPB on the barricade.

4.3. *Effect of slurry concentrations*

Fig. 17 indicates the impact of diverse solid contents on barricade's lateral pressure. With rising fill solid contents, lateral stress on barricade rises as a whole, and the peak value is especially obvious, which indicates that when using the means of increasing concentration to improve fill's strength, it is required to consider barricade's strength to withstand the increasing lateral pressure, and if the concentration is increased too much, it may cause accidents such as barricade collapse. If a higher filling slurry concentration is used, the thickness of the barricade needs to be increased.

Although solid content is different, the trend of pressure change is

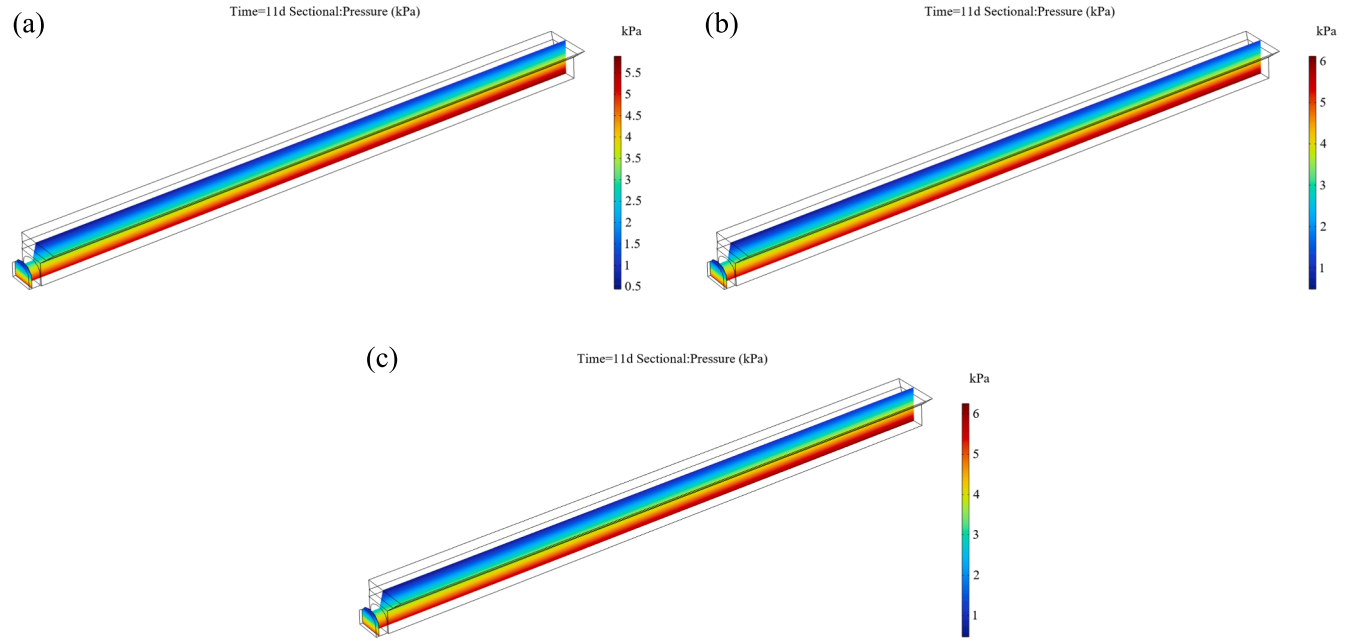

Fig. 18. Pressure distribution inside CPB with different filling slurry contents: (a) 66%; (b) 68%; (c) 70%.

basically the same, the trend is that with rising time, pressure rises first, reaches peak and then gradually reduces and tends to stabilize. Fig. 18 demonstrates the pressure distribution inside CPB. Because change's mass concentration is similar, change in the longitudinal section of the figure below is not very obvious.

5. Conclusions

To accurately grasp the change rule of lateral stress on barricade during fill, This paper presents the establishment of a numerical model that considers the response of the barricade to the THMC coupling process of the CPB during the long-term continuous filling process. The model considers the hydration process of the cementitious material, the generation and transfer of heat, the evolution of pore pressure, and the mechanical processes occurring within the system. It also adopts field monitoring data to link with estimate outcomes of numerical model, the effect of lateral pressure on barricade under different filling conditions is investigated. The following conclusions are reached:

(1) Constructed mathematical model can characterize the behavior of CPB coupled THMC, and model's validity and analytical ability is confirmed by simulating mechanical influence of fill retaining wall and variation of internal heat field of CPB in comparison with the actual monitoring situation. The model can be used to further study the change of lateral pressure of barricade under different working conditions.

(2) Barricade is considerably governed through coupling practices occurring in the backfill. At the beginning of filling, CPB generates stress on barricade in loose fluid form, and stress on barricade rises and then losses, and lastly tends to stabilize. As fill's curing time reaches a certain stage, CPB at the bottom will form a certain stability to endure upper stress, so that pressure at barricade will be reduced.

(3) The placement of barricade has obvious influence for the lateral pressure on barricade. At the later stage of curing, the lower portion of CPB exhibits a cemented state, when space between barricade and stope rises, pressure on barricade will be reduced, in instances where the distance between the barricade and the stope exceeds three times the height of the former, the barricade is deemed to be unaffected by the local load. so in the process of designing the barricade structure, the placement of barricade should be fully considered.

(4) Fill's initial heat has a major effect on barricade's lateral pressure, and a greater initial heat can quicken hydrated reaction inside CPB, the requisite time for CPB consolidation is reduced, thereby facilitating the formation of a self-stable state, such as, microwave heating curing and other new curing methods, and the time when the lateral pressure of barricade reaches its peak will be further shortened. Hence, appropriate heating measures can be applied to CPB to rise fill's initial temperature, accelerate fill's curing rate so that it can quickly form early strength and relieve the pressure on the barricade.

(5) Lateral stress exerted on barricade varies with fill's diverse concentrations. When fill's solid content increases, the pressure on barricade increases accordingly. Therefore, when considering the usage of increased concentration to augment fill's strength, it is crucial to assess whether the barricade can withstand the increased lateral pressure.

While a numerical model is developed for analyzing the response process of the barricade to the CPB coupling behavior in this paper, the application of the model is constrained. For instance, the impact of stope dimensions and configuration on the lateral pressure evolution of a barricade is not addressed. Accordingly, future research will further examine the behavior of the barricade in consideration of the interaction between CPB and stope. Moreover, the model is anticipated to be expanded to encompass the design of more stable barricade.

CRediT authorship contribution statement

Di Wu: Writing – review & editing, Supervision, Methodology. **Liang Liu:** Writing – original draft, Investigation, Conceptualization. **Erol Yilmaz:** Writing – review & editing, Visualization, Resources, Methodology. **Shilong Zheng:** Writing – review & editing, Methodology, Investigation.

Declaration of competing interest

The authors declare that they have no known competing financial interests or personal relationships that could have appeared to influence the work reported in this paper.

Acknowledgements

The present research was generously funded by the National Key

Research and Development Program of China (2022YFC2905600) and the National Natural Science Foundation of China (52374110). This study has been supported by the Recep Tayyip Erdoğan University Development Foundation (Grant number: 02024008021039). The supports granted are gratefully acknowledged to the relevant research fund bodies.

References

[1] M. Jiang, S. Cao, E. Yilmaz, Analyzing microscopic structure and macroscopic strength behavior of cement-based tail fills incorporating fiber by X-ray CT scanning technique, Constr. Build. Mater. (2024).
[2] G. Lu, M. Fall, Modeling postblasting stress and pore pressure distribution in hydrating fill mass at an early age, Int. J. Geomech. 18 (2018) 04018090, https://doi.org/10.1061/(ASCE)GM.1943-5622.0001141.
[3] N. Sivakugan, K. Rankine, R. Rankine, Permeability of Hydraulic Fills and Barricade Bricks, Geotech. Geol. Eng. 24 (2006) 661–673, https://doi.org/10.1007/s10706-005-2132-8.
[4] F.Z. Wang, I.L. Animasaun, D.M. Al Shamsi, T. Muhammad, A. Ali, Transient cold-front-water through y-shaped aluminium ducts: nature of turbulence, non-equilibrium thermodynamics, and velocity at the converged and diverged outlets, J. Non-Equil. Thermody. 485 (2024).
[5] M. Fall, O. Nasir, Mechanical behaviour of the interface between cemented tailings backfill and retaining structures under shear loads, Geotech. Geol. Eng. 28 (2010) 779–790, https://doi.org/10.1007/s10706-010-9338-0.
[6] J. Zheng, L. Li, Experimental study of the “short-term” pressures of uncemented paste backfill with different solid contents for barricade design, J. Clean. Prod. 275 (2020) 123068, https://doi.org/10.1016/j.jclepro.2020.123068.
[7] N. Abdul-Hussain, M. Fall, M. Saatcioglu, Blast response of cantilever retaining wall: Modes of wall movement, Transp. Geotech. 40 (2023) 100950, https://doi.org/10.1016/j.trgeo.2023.100950.
[8] L. Cui, M. Fall, Modeling of pressure on retaining structures for underground fill mass, Tunn. Undergr. Space Technol. 69 (2017) 94–107, https://doi.org/10.1016/j.tust.2017.06.010.
[9] M. Azree Othuman Mydin, N. Hamah Sor, A. Bahrami, A. Dulaimi, Y. Onuralp Özkılıç, F. Althoey, P. Jagadesh, H.F. Isleem, T.A. Tawfik, Residual durability, mechanical, and microstructural properties of foamed concrete subjected to various elevated temperatures, Eng. Sci. Technol. Int. J. 55 (2024) 101725, https://doi.org/10.1016/j.jestch.2024.101725.
[10] T.G.G. Molay, M.N.L. Leroy, T. Fidele, H.G. Franck, N.-J.-M. Bienvenu, Mechanical and physical performances of concretes made from crushed sands of different geological nature subjected to high temperatures, Eng. Sci. Technol. Int. J. 22 (2019) 1116–1124, https://doi.org/10.1016/j.jestch.2019.02.007.
[11] F. Wang, I.L. Animasaun, Q.M. Al-Mdallal, S. Saranya, T. Muhammad, Dynamics through three-inlets of t-shaped ducts: significance of inlet velocity on transient air and water experiencing cold fronts subject to turbulence, Int. Commun. Heat Mass Transf. 148 (2023) 107034, https://doi.org/10.1016/j.icheatmasstransfer.2023.107034.
[12] J. Qin, J. Zheng, L. Li, An analytical solution to estimate the settlement of tailings or backfill slurry by considering the sedimentation and consolidation, Int. J. Min. Sci. Technol. 31 (2021) 463–471, https://doi.org/10.1016/j.ijmst.2021.02.004.
[13] S. Etli, T. Yılmaz, O. Hansu, Effect of White-Portland cement containing micro and nano silica on the mechanical and freeze-thaw properties of self compacting mortars, Eng. Sci. Technol. Int. J. 50 (2024) 101614, https://doi.org/10.1016/j.jestch.2023.101614.
[14] S. An, J. Liu, L. Cheng, L. Guo, D. Zhou, Rheological and mechanical properties of full-tailings backfill material prepared by ultrafine-iron-tailings-powder-based consolidation agent, Constr. Build. Mater. 417 (2024) 135286, https://doi.org/10.1016/j.conbuildmat.2024.135286.
[15] F.Z. Wang, I.L. Animasaun, T. Muhammad, S.S. Okoya, Recent advancements in fluid dynamics: drag reduction, lift generation, computational fluid dynamics, turbulence modelling, and multiphase flow, Arab. J. Sci. Eng. 49 (2024) 10237–10249, https://doi.org/10.1007/s13369-024-08945-3.
[16] Z. Wang, Y. Wang, M. Zhang, A. Wu, Z. Ruan, G. Yu, Effect of curing pressure on the stability of bottom cemented paste backfill under different types of barricade, Case Stud. Constr. Mater. 18 (2023) e01732, https://doi.org/10.1016/j.cscm.2022.e01732.
[17] Y. Zhai, An update of the 3D analytical solution for the design of barricades made of waste rocks, Int. J. Rock Mech. Min. Sci. 158 (2022) 105176, https://doi.org/10.1016/j.ijrmms.2022.105176.
[18] Y. Zhai, P. Yang, L. Li, Analytical solutions for the design of shotcreted waste rock barricades to retain slurried paste backfill, Constr. Build. Mater. 307 (2021) 124626, https://doi.org/10.1016/j.conbuildmat.2021.124626.
[19] M. Nujaim, T. Belem, A. Giraud, Experimental tests on a small-scale model of a mine stope to study the behavior of waste rock barricades during backfilling, Minerals 10 (2020) 941, https://doi.org/10.3390/min10110941.
[20] L. Li, I.L. Animasaun, O.K. Koriko, T. Muhammad, T. Elnaqeeb, Insight into turbulent Reynolds number at the regular, converging, and diverging outlets: dynamics of air, water, and kerosene through y-shaped cylindrical copper ducts, Int. Commun. Heat Mass Transf. 159 (2024) 108044, https://doi.org/10.1016/j.icheatmasstransfer.2024.108044.
[21] Y. Wang, Q. Na, J. Yang, L. Zhang, J. Zhang, J. Li, F. Jin, Monitoring of barricade pressure during the entire backfilling process for a high iron mine stope, Case Stud. Constr Mater (2023).
[22] B.D. Thompson, W.F. Bawden, M.W. Grabinsky, In situ measurements of cemented paste backfill at the Cayeli Mine, Can. Geotech. J. 49 (2012) 755–772, https://doi.org/10.1139/t2012-040.
[23] J.P. Doherty, A. Hasan, G.H. Suazo, A. Fourie, Investigation of some controllable factors that impact the stress state in cemented paste backfill, Can. Geotech. J. 52 (2015) 1901–1912, https://doi.org/10.1139/cgj-2014-0321.
[24] Y. Wang, Q. Na, L. Zhang, Monitoring of in-situ properties for cemented tailings backfill that under drainage condition, Constr. Build. Mater. 356 (2022) 129254, https://doi.org/10.1016/j.conbuildmat.2022.129254.
[25] M. Sheikholeslami, Z. Khalili, Enhancing photovoltaic solar panel performance with integration of PCM-based spectral filter and self-cleaning coating, J. Build. Eng. 94 (2024) 110019, https://doi.org/10.1016/j.jobe.2024.110019.
[26] D.V.H. Teja, P. Muvvala, N.A. Prashanth Nittala, D. Bandhu, M.I. Khan, K. K. Saxena, M.I. Khan, Comparative performance analysis of recuperative helium and supercritical CO_2 Brayton cycles for high-temperature energy systems, Energy 312 (2024) 133469, https://doi.org/10.1016/j.energy.2024.133469.
[27] D. Wu, M. Fall, S.J. Cai, Coupling temperature, cement hydration and rheological behaviour of fresh cemented paste backfill, Miner. Eng. 42 (2013) 76–87, https://doi.org/10.1016/j.mineng.2012.11.011.
[28] A. Ghirian, M. Fall, Coupled thermo-hydro-mechanical–chemical behaviour of cemented paste backfill in column experiments, Eng. Geol. 170 (2014) 11–23, https://doi.org/10.1016/j.enggeo.2013.12.004.
[29] S. Poyet, S. Charles, N. Honoré, V. L’hostis, Assessment of the unsaturated water transport properties of an old concrete: determination of the pore-interaction factor, Cem. Concr. Res. 41 (2011) 1015–1023, https://doi.org/10.1016/j.cemconres.2011.06.002.
[30] L. Cui, M. Fall, An evolutive elasto-plastic model for cemented paste backfill, Comput. Geotech. 71 (2016) 19–29, https://doi.org/10.1016/j.compgeo.2015.08.013.
[31] L. Cui, M. Fall, A coupled thermo–hydro-mechanical–chemical model for underground cemented tailings backfill, Tunn. Undergr. Space Technol. 50 (2015) 396–414, https://doi.org/10.1016/j.tust.2015.08.014.
[32] D. Wu, W. Hou, S. Liu, H. Liu, Mechanical response of barricade to coupled THMC behavior of cemented paste backfill, Int. J. Concr. Struct. Mater. 14 (2020) 39, https://doi.org/10.1186/s40069-020-00413-0.
[33] D. Wu, W. Hou, H. Yang, L. Guo, Numerical analysis of the hydraulic and mechanical behavior of in situ cemented paste backfill, Geotech. Geol. Eng. 38 (2020) 4877–4887, https://doi.org/10.1007/s10706-020-01333-2.
[34] G. Sulochana, C.V. Prasad, S.K. Bhatti, V.V. Venu Madhav, K.K. Saxena, M.I. Khan, Z. Aloui, C. Prakash, M.I. Khan, Impact of multi-walled carbon nanotubes (MWCNTs) on hybrid biodiesel blends for cleaner combustion in CI engines, Energy 303 (2024) 131911, https://doi.org/10.1016/j.energy.2024.131911.
[35] T.-H. Zhao, M.I. Khan, S. Qayyum, R. Naveen Kumar, Y.-M. Chu, B. C. Prasannakumara, Comparative study of ferromagnetic hybrid (manganese zinc ferrite, nickle zinc ferrite) nanofluids with velocity slip and convective conditions, Phys. Scr. 96 (2021) 075203, https://doi.org/10.1088/1402-4896/abf26b.
[36] P. Navi, C. Pignat, Simulation of cement hydration and the connectivity of the capillary pore space, Adv. Cem. Based Mater. 4 (1996) 58–67, https://doi.org/10.1016/S1065-7355(96)90052-8.
[37] S. Han, Y. Liu, Y. Lyu, J. Liu, N. Zhang, Numerical simulation investigation on hydration heat temperature and early cracking risk of concrete box girder in cold regions, (n.d.).
[38] K. Fang, M. Fall, L. Cui, Thermo-chemo-mechanical cohesive zone model for cemented paste backfill-rock interface, Eng. Fract. Mech. 244 (2021) 107546, https://doi.org/10.1016/j.engfracmech.2021.107546.
[39] D. Wu, Y. Hou, T. Deng, Y. Chen, X. Zhao, Thermal, hydraulic and mechanical performances of cemented coal gangue-fly ash backfill, Int. J. Miner. Process. 162 (2017) 12–18, https://doi.org/10.1016/j.minpro.2017.03.001.
[40] B. Yan, R. Wang, B. Ding, F. Dai, Y. Wang, Numerical simulation analysis of tunnel backfill grout based on DEM-FDM coupling and particle inlet, Undergr. Space 14 (2024) 285–299, https://doi.org/10.1016/j.undsp.2023.06.004.
[41] D. Wu, M. Fall, S. Cai, Numerical modelling of thermally and hydraulically coupled processes in hydrating cemented tailings backfill columns, Int. J. Min. Reclam. Environ. 28 (2014) 173–199, https://doi.org/10.1080/17480930.2013.809194.
[42] J.P. Doherty, A numerical study into factors affecting stress and pore pressure in free draining mine stopes, Comput. Geotech. 63 (2015) 331–341, https://doi.org/10.1016/j.compgeo.2014.10.001.
[43] M.T. Van Genuchten, A closed-form equation for predicting the hydraulic conductivity of unsaturated soils, Soil Sci. Soc. Am. J. 44 (1980) 892–898, https://doi.org/10.2136/sssaj1980.03615995004400050002x.
[44] A.M. Al-Swaidani, S.D. Aliyan, N. Adarnaly, Mechanical strength development of mortars containing volcanic scoria-based binders with different fineness, Eng. Sci. Technol. Int. J. 19 (2016) 970–979, https://doi.org/10.1016/j.jestch.2015.12.006.
[45] Z. Aldhafeeri, M. Fall, M. Pokharel, Z. Pouramini, Temperature dependence of the reactivity of cemented paste backfill, Appl. Geochem. 72 (2016) 10–19, https://doi.org/10.1016/j.apgeochem.2016.06.005.
[46] M. Fall, J.C. Célestin, M. Pokharel, M. Touré, A contribution to understanding the effects of curing temperature on the mechanical properties of mine cemented

tailings backfill, Eng. Geol. 114 (2010) 397–413, https://doi.org/10.1016/j.enggeo.2010.05.016.
[47] M. Ziada, S. Erdem, R. Alonso González-Lezcano, Y. Tammam, İ. Unkar, Influence of various fibers on the physico-mechanical properties of a sustainable geopolymer mortar-based on metakaolin and slag, Eng. Sci. Technol. Int. J. 46 (2023) 101501, https://doi.org/10.1016/j.jestch.2023.101501.
[48] M.M. Hilles, M.M. Ziara, Mechanical behavior of high strength concrete reinforced with glass fiber, Eng. Sci. Technol. Int. J. 22 (2019) 920–928, https://doi.org/10.1016/j.jestch.2019.01.003.